Indonesian Journal of Electrical Engineering and Computer Science
Vol. 32, No. 1, October 2023, pp. 107~113
ISSN: 2502-4752, DOI: 10.11591/ijeecs.v32.i1.pp107-113

Green-emitting $YBO_3:Ce^{3+},Tb^{3+}$ phosphor photoluminescence characteristics for close UV stimulation

Ho Minh Trung[1], My Hanh Nguyen Thi[2], Nguyen Le Thai[3]
[1]Faculty of Basic Sciences, Vinh Long University of Technology Education, Vinh Long, Vietnam
[2]Faculty of Mechanical Engineering, Industrial University of Ho Chi Minh City, Ho Chi Minh City, Vietnam
[3]Faculty of Engineering and Technology, Nguyen Tat Thanh University, Ho Chi Minh City, Vietnam

Article Info

Article history:

Received Sep 7, 2022
Revised Jul 14, 2023
Accepted Jul 17, 2023

Keywords:

Color homogeneity
Double-layer phosphor
Luminous flux
Monte carlo theory
WLEDs

ABSTRACT

Through a solid state process, $YBO_3:Ce^{3+},Tb^{3+}$ was created via rare earth oxides along with boric acid. The phosphor absorbs close-ultraviolet illumination through the transitions 4f-5d of Ce^{3+}, then emits a wide spectrum of light through the transitions 5d-4f of Ce^{3+} and a sharp spectrum of light through the transitions 4f-4f of Tb^{3+}. Nonradioactive power transmission between Ce^{3+} and Tb^{3+} has been seen in samples with varying amounts of Ce^{3+} and Tb^{3+} using spectroscopic analysis. The quantities of Ce^{3+} as well as Tb^{3+} decides the hue for the $YBO_3:Ce^{3+},Tb^{3+}$ emission, ranging between blue and green. The $Y_{0.82}Ce_{0.03}Tb_{0.15}BO_3$ phosphor, which emits green light when optimized, has an exterior quantum effectiveness of 76.7% and an emission color of (0.309, 0.547). This phosphor's luminescence strength maintains 87% of its strength at ambient temperature, demonstrating enough heat stability for white illumination emitting diode implementations.

Corresponding Author:

My Hanh Nguyen Thi
Faculty of Mechanical Engineering, Industrial University of Ho Chi Minh City
No. 12 Nguyen Van Bao Street, Ho Chi Minh City, Vietnam
Email: nguyenthimyhanh@iuh.edu.vn

1. INTRODUCTION

One of the crucial areas for study in the realm of electrochemistry has been the investigation of innovative phosphor substances [1], [2]. As wavelength converters for diodes emit white illumination (LEDs), phosphors that release visible colors when excited by blue or close UV illumination have received a lot of interest recently. The first white LED to be sold in stores is made up of one blue LED along with a $Y_3A_{l5}O_{12}$(YAG):Ce^{3+} sample capable of changing the wavelength of blue illumination to yellow illumination. To increase the hue rendering index of white illumination, a close UV LED along with red, green, blue (RGB) phosphor samples have been combined [3], [4]. Recent studies had concerned sulfide phosphor samples, such as $ZnS:Cu^{+},Al^{3+}$ as well as $SrGa_2S_4:Eu^{2+}$, in order to achieve an effective wavelength conversion from close UV to green illumination, even if their chemical stability is insufficient for practical purposes [5]–[7]. Due to their high quantum effectiveness, broad stimulating wavelength range from the UV to the blue area, and strong chemical and heat stabilities, oxynitride phosphor samples incorporated with Eu^{2+} can be produced in the form of effective green phosphor samples. They can only be produced using high heat processes between 1,300 and 2,000 °C, though. Other green-emitting phosphors with equivalent characteristics and kinder preparation requirements must yet be found [8].

From the perspectives of great chemical and heat stability and excellent optic transparency in the close UV and viewable areas, yttrium borate would be an appropriate crystal base to house phosphors. There are several ways to synthesize YBO_3, involving wet chemical approaches at lower temperatures as well as solid state processes that take place between 1,000 and 1,200 °C [9]. For use in plasma display panel applications,

several studies have described the synthesis and characterisation for $YBO_3:Eu^{3+}$ as well as $YBO_3:Tb^{3+}$ having varied magnitudes as well as forms. We recently published a hydthermal combination of $YBO_3:Ce^{3+}$, a phosphor that emits blue light when excited by close UV radiation [10], [11].

In many different forms for non-organic phosphor samples, the trivalent Ce^{3+} ion serves as an effective luminous center substitution. By transferring energy from Ce^{3+} to Tb^{3+}, Ce^{3+} becomes one responsitizer in the case of one Tb^{3+} granules that emits green light, such as $LaPO_4:Ce^{3+},Tb^{3+}$. Ce^{3+} generally exhibits a wide absorption across the spin- and parity-allowed conversion from the stimulated $4f^0 5d1$ state to the ground 4f1 state [12], [13]. The crystalline cleavage for the 5d states, which is controlled by the crystal base's layout, has a significant impact on the energy of this absorption photon. By selecting an appropriate base, we can adjust the stimulation wavelength for Ce^{3+} between the UV and the blue area. When it comes to YBO_3 of the vaterite kind, Ce^{3+} ion takes the place of Y^{3+} and exhibits a widespread absorptivity in the close UV area at ~365 nm.

The study herein concerns YBO_3 dually incorporated with Ce^{3+} as well as Tb^{3+} in the form of one new, near-UV-excited, green-emitting phosphor. Many studies discovered on their preliminary findings into the photoluminescence (PL) of the $YBO_3:Ce^{3+},Tb^{3+}$. To our understanding, though, there have not yet been any thorough analyses of the PL characteristics of $YBO_3:Ce^{3+},Tb^{3+}$, including the effects of Ce^{3+} as well as Tb^{3+} dosages upon PL strengths, ideal Ce^{3+} as well as Tb^{3+} dosages, luminous quantum effectiveness, along with emitting hue [14], [15]. This research aims to reveal the PL characteristics for $YBO_3:Ce^{3+},Tb^{3+}$ utilizing specimens of $Y_{1-x-y}Ce_xTb_yBO_3$ produced by a solid state synthesis and having varying Ce^{3+} and Tb^{3+} concentrations. We further look at how the PL strength varies with temperature and talk about the prospect of using $YBO_3:Ce^{3+},Tb^{3+}$ when it comes to WLED implementations.

2. METHOD

The similar spectrometer with an integrating sphere unit was used to evaluate absolute external quantum efficiency (EQE), which was calculated utilizing the (1) [16]:

$$EQE = \frac{I_{em}}{I_{ex} - I_{ref}} \tag{1}$$

where I_{em} stands for the sample's integrated emitting strength, I_{ex} for the stimulation illumination that strikes the sample directly, and I_{ref} for the stimulation light that is not absorbed by the specimen. I_{ex} was measured using a reflectance standard. At heats ranging from ambient temperature to 300 °C, PL spectra were measured using a heating attachment.

When nonradiative energy is transferred from a donor to an acceptor, the power transmission effectiveness, or η_{ET}, is given by (2) [17]:

$$\eta_{ET} = 1 - \frac{\eta}{\eta_0} \tag{2}$$

η_0 and η signify the quantum productivities for the giving radiation when not accompanied by the acceptor and in the existence of the receiver, in turn. The η_{ET} outcomes for $Y_{0.97-y}Ce_{0.03}Tb_yBO_3$ specimens were computed then displayed in the form of one function for Tb^{3+} dosage, utilizing an estimate that it is possible to supplant the proportion η/η_0 using the proportion for incorporated PL strengths. The η_{ET} value steadily rises as Tb^{3+} dosage raises, indicating a steadily rising likelihood for power conversion between Ce^{3+} and Tb^{3+}. The critical dosage for Tb^{3+}, or the dosage rendering the possibility for power conversion between excited Ce^{3+} and Tb^{3+} equivalent to the possibility for attenuation pathways, η_{ET}=0.5, is 3.2 at %.

The (3) and (4) could be used to calculate the critical spaces for dipole-dipole as well as dipole-quatrupole interactivities [18]:

$$R_{dd}{}^6 = \frac{3\hbar^4 c^4 Q_a}{4\pi n^4} \int \frac{f_d(E) F_a(E)}{E^4} dE \tag{3}$$

$$R_{dq}{}^8 = \frac{3\hbar^4 c^4 f_q \lambda_s^2 Q_a}{4\pi n^4 f_d} \int \frac{f_d(E) F_a(E)}{E^4} dE \tag{4}$$

the (5) may be used to calculate the dopant ions' mean closest neighbor distance [19], R:

$$R \approx 2\left(\frac{3V}{4\pi CN}\right)^{1/3} \tag{5}$$

where V is the unit cellule's volume, C signifies the doping dosage. N signifies the total amount for dopant ion-accepting locations. Utilizing said factors, being the total dosage for Ce^{3+} as well as Tb^{3+}, the R value is

predicted to be 11.9 Å judging the critical dosage stated before, i.e., Ce^{3+} reaching 3.0 at %, Tb^{3+} reaching 3.2 at %. The real mean distance among one Ce^{3+} granule and a closest adjacent Tb^{3+} granule would be therefore exceeds 11.9 Å. It is significant to mention that the critical distances of the three power transmission processes are bigger than the mean closest adjacent range among Ce^{3+} as well as Tb^{3+} under the critical dosage. This may be explained by the fact that the high Ce^{3+} concentration prevents stimulated power migration among Ce^{3+} ions from becoming inconsequential in the energy transmission procedure. A same phenomenon was noted in the $CeBO_3$:Tb^{3+} layout by Blasse and Bril [20], [21].

3. RESULTS AND DISCUSSION

The optimal light source for general illumination needs to have the highest luminous efficacy of radiation (LER) and excellent color rendering. While it is clear how to compute the LER, there is still disagreement on what constitutes "excellent" color rendering [22]. The chroma rendition index (CRI), or hue rendering index, is the current industry standard for hue rendering. The Commission Internationale de l'Eclairage (CIE) developed the index in 1965, updated it in 1974, and reissued in 1995 with small modifications. It is helpful to condense the meaning for said index. A book by Schanda concerns a comprehensive overview on this index. Color rendering index (CRI) is defined based on a comparison of the test items' colors under the test light source and their colors under a reference supply. The selection of this example is obviously crucial since it establishes what the 'real' hues of items are.

Judging the the kind of testing means, an infinite quantity for referential supplies is employed for defining the index: The test source's correlated color temperature (CCT) would be determined through first collating the source’s spectrum to that of one black body radiator [23]. The heat of the black body that most nearly links the test means's spectrum is then determined. When the test source's CCT goes below 5,000 K, one black body radiator having the same CCT serves as the referential source to determine CRI. Exceeding 5,000 K, a standard daylight spectrum with the identical CCT that was created using the CIE's D65 standard illuminant is utilized. It is obvious that researchers have extensively researched the wide range producing rare earth ions Eu^{2+} and Ce^{3+}. This is mainly due to their distinctive emission characteristics, which combine a broad emission spectrum (resulting in strong hue rendering qualities), a very modest Stokes shift (enabling excitation within the close-UV or blue spectral section), along with quick decomposition durations (avoiding saturation).

High quantum performances and a favorable heating quenching behavior can be attained depending on the host material. Moreover, by carefully selecting the host molecule, it is possible to adjust the emitting spectrum between close-UV and deep red. One spin orbit with two levels ($^2F_{5/2}$ and $^2F_{7/2}$), and a power division of around 2000 cm^{-1}, may be seen in the 4f ground state. The lowest 5d excited state is reduced in power, or red-shifted, when incorporated into an inorganic molecule as opposed to the free (gaseous) Ce^{3+} ion. The crystal field splitting and centroid shift that make up this red-shift are caused by the nephelauxetic effect, which is dependent on the polarizability of the nearby anions. Therefore, it is possible to alter the emission and excitation wavelengths by varying the host material's composition. The Stokes shift, which is the dissimilarity among the absorptivity and emitting power, results from lattice relaxation following the stimulation of the 4f electron to the 5d orbital (a similar relaxation also happens after the transition to the ground state). Due of the shifts between the 5d stimulated status and spin orbit split ground status, Ce^{3+} exhibits a wide emission spectrum.

Similar figures can be produced after doping with Eu^{2+}, with the major distinction being that the $4f^7$ ground state is a single level ($^8S_{7/2}$), meaning that spin orbit splitting is absent, and the emitting spectrum is essentially made up of a sole emitting range with a figurative FWHM in the 50–100 nm range. The presence of many emission bands in some substances might cause the emission spectrum to widen. When the Eu-ions are integrated on lattice sites with distinct symmetry and/or a distinctly space from the nearest neighbor ions, this effect is seen. In general, monovalent or divalent cation sites where Eu^{2+} is present allow for the observation of Eu^{2+} emission. Owing to the 5d excited state's location in the host's conduction range, Eu^{2+} radiation is seldom seen when a trivalent ion is substituted for it.

Owing to the splitting of the 5d recreated state via the crystalline field, coupled to the multiplet splitting of the $4f^6$ structure, the excitation spectrum for compounds with Eu^{2+} doping is wide and frequently quite featureless. The latter is comparable to the ^7F_J level ground state splitting for Eu^{3+}, which can occasionally result in a staircase-like fine layout in the stimulation spectra. With close-UV as well as blue LEDs, a great overlap would be attainable with phosphor samples generating discharge between green and red. With Ce^{3+} as the main exception, most trivalent rare earth ions produce a series of rather narrow emission lines as a result of intrinsic $4f^n$ -$4f^n$ conversions that are scarcely influenced by the host molecule. The host does, however, have little impact on the emissive characteristics of these 4f-4f emitters because it affects the quantum performance (due to the presence of non-radiative pathways and heat quenching behavior) as well as the relative strength of the emitting lines (via choosing rules related to local symmetry). A lot of these rare earth ions release illumination that may be seen. Notable rare earth ions include Tb^{3+} (green radiation, reach the apex under 545 nm) along with Eu^{3+} (radioactivity between orange and red, reach an apex almost 600 or 620 nm),

which have both been extensively used in cathode ray tubes and fluorescent light phosphors. Since 5d states as well as charge shift statuses (CSS) would be usually found much below 350 nm (as indicated for $Y_2O_2S:Eu^{3+}$), the main challenge with converting these substances to LED applications is the absence of effective, broad range recreation paths between the close-UV and blue spectral section [24].

Figure 1 illustrates the reversal of the relationship between the concentrations of green phosphorus $YBO_3:Ce^{3+},Tb^{3+}$ as well as phosphorus $YAG:Ce^{3+}$. Said adjustment maintains median CCT levels, and affects the absorption as well as disspersion for two phosphor sheets in WLEDs. In the end, this affects how well WLEDs perform in terms of luminous flux and color quality. Thus, the selection of the $YBO_3:Ce^{3+},Tb^{3+}$ concentration aletrs the chroma output in WLED apparatuses. As the $YBO_3:Ce^{3+},Tb^{3+}$ dosage climbed (2-20% wt), it declined, sustaining the average CCTs. The same is valid for WLEDs that have disparate chroma heat levels ranging between 5,600 and 8,500 K.

Figure 2 makes it clear how the $YBO_3:Ce^{3+},Tb^{3+}$ presence affects the transmission spectrum in the WLED apparatus. One can select options according to the specifications set out by the manufacturer. Low luminous flux WLEDs can be used when great color fidelity is required. Figure 2 illustrates how the spectral band that makes up white light is combined. These five images each show a spectrum at a different color temperature: 5,600 K, 6,600 K, 7,000 K, 7,700 K, along with 8,500 K. The potency escalates alongside the dosages of $YBO_3:Ce^{3+},Tb^{3+}$ within specific spectral areas, 420 nm–480 nm as well as 500 nm–640 nm. A growth for the yielded illumination is indicated by the dual-band emitting spectra, which has increased. On the other hand, judging the WLEDs' superior blue-illumination dispersion, the dual phosphor sheets along with the greater dispersion in WLED augments chroma consistency, which is a significant result. Managing the chroma consistency for the remote phosphor setting at high heats would be hard. The paper herein shows that $YBO_3:Ce^{3+},Tb^{3+}$ may enhance the hue standard of WLEDs at both high and low hue heats (5,600 K and 8,500 K).

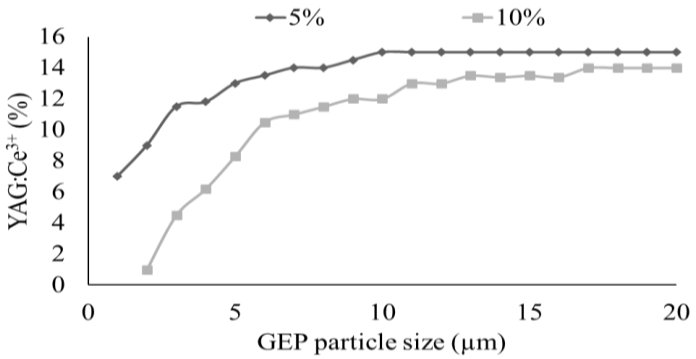

Figure 1. Changing phosphor presence for retaining average CCT

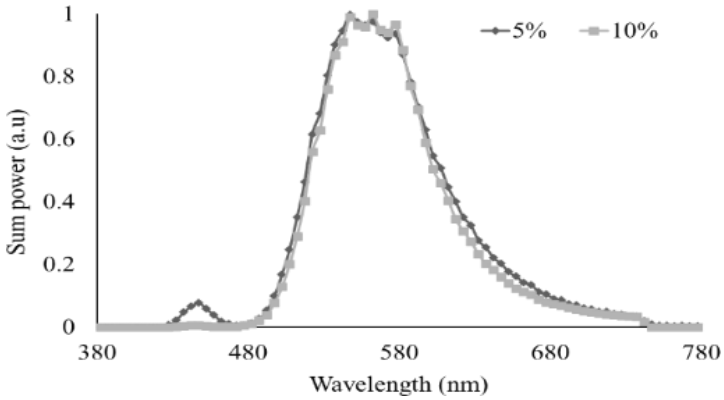

Figure 2. The discharging spectra in 4,000 K WLED device correlating with $YBO_3:Ce^{3+},Tb^{3+}$ presence

The study herein manages to prove the efficiency for the two-sheet illumination discharge in remote phosphor setting. Judging Figure 3, as $YBO_3:Ce^{3+},Tb^{3+}$ dosage escalated (2–20%), the lumen surged

substantially. Judging every CCT level in Figure 4, the $YBO_3:Ce^{3+},Tb^{3+}$ concentration greatly decreased the color deviation, possibly resulting from the absorption from the red sheet of phosphor. If $YBO_3:Ce^{3+},Tb^{3+}$ assimilates the blue illumination generated via the LED chip, it converts it into green llumination, subsequently generated via granules of blue phosphor. The $YBO_3:Ce^{3+},Tb^{3+}$ particles also continue to assimilate yellow light. Nonetheless, the blue illumination absorption would be larger, a result of the substance's absorption qualities. With the addition of $YBO_3:Ce^{3+},Tb^{3+}$, the green-illumination concentration in the WLED device increases, which boosts the hue consistency. This factor would be among the most necessary features. The WLED cost surges as the chroma consistency rises. On the other hand, the inexpensive price for $YBO_3:Ce^{3+},Tb^{3+}$ is a benefit. $YBO_3:Ce^{3+},Tb^{3+}$ can therefore be applied broadly.

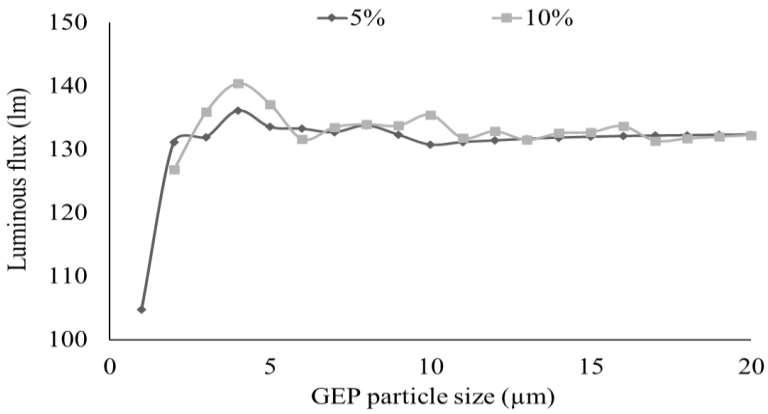

Figure 3. The illumination for WLED device correlating with $YBO_3:Ce^{3+},Tb^{3+}$ presence

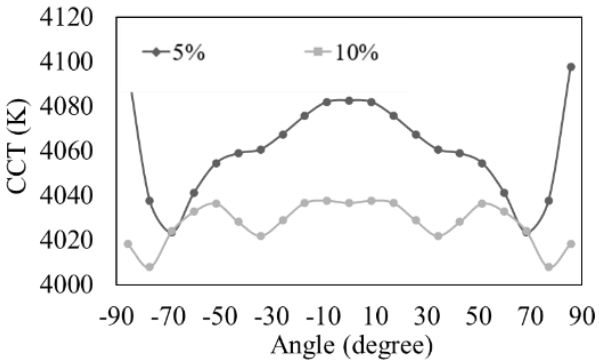

Figure 4. CCT in WLED device correlating with $YBO_3:Ce^{3+},Tb^{3+}$ presence

Chroma consistency would simply be one of many factors for gauging the WLEDs' chroma quality [25], [26]. Significant hue consistency does not guarantee a decent hue standard. Hence, it is necessary to utilize CRI ans chroma quality scale (CQS). CRI shows entities' true chroma if they are illuminated. If green illumination becomes excessive among the key chromas (green, yellow, blue), there will be an imbalance in the chroma gamut, aletring the color precision of WLEDs, leading to inferior chroma quality. Figure 5 displays one slight CRI drop when the distant phosphor $YBO_3:Ce^{3+},Tb^{3+}$ layer is present. However, given that CRI would be only one drawback for CQS, this event would be acceptable. The challenge in CQS obtainment would surpass CRI [27]. Three variables combine to form the CQS index: the color rendering index comes in first, followed by viewer preference and hue coordinate. About these three essential elements, CQS comes close to being a real overall evaluation for chroma output. Figure 6 displays how CQS is enhanced when the phosphor $YBO_3:Ce^{3+},Tb^{3+}$ layer is introduced [28]. Additionally, the CQS does not change much as the $YBO_3:Ce^{3+},Tb^{3+}$ concentration is raised when it is less than 10% wt. The substantial hue loss when green is prevalent results in CRI as well as CQS highly declined under $YBO_3:Ce^{3+},Tb^{3+}$ dosage exceeding 10% wt. Hence, picking a suitable dosage is a must.

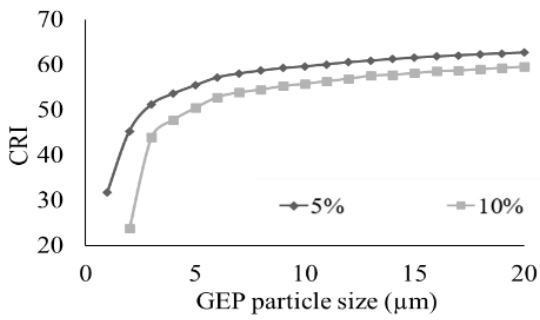

Figure 5. CRI in WLED device correlating with $YBO_3:Ce^{3+},Tb^{3+}$ presence

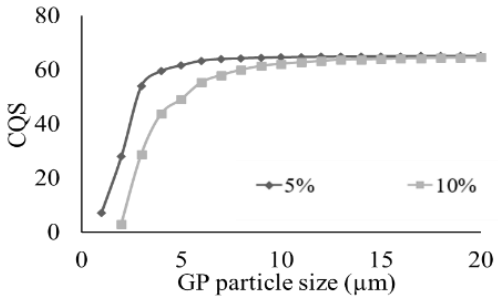

Figure 6. CQS in WLED device correlating with $YBO_3:Ce^{3+},Tb^{3+}$ presence

4. CONCLUSION

It is obvious that a range of doping elements can be used for creating good conversion phosphor samples based on the required kind of emission spectrum. The base latticework has to adhere to specific criteria. It should go without saying that the base has to have high thermal as well as chemical robustness so that it can withstand the high heat levels near the LED chip, achieving the prolonged durability. Additionally, the matter has to have optical transparency to the light being produced. The base has to remain clear in the case of the radiation of the LED unless a host-dopant power conversion takes place, which restricts the options to broad band-gap substances. If the replaced ion and the dopant ion in the host do not have any charge or size differences, incorporating dopants into the host substance is made easier. With regard to the thermal input, the gases and precursors utilized, and last but not least, affordability, environmentally friendly practices should be used when producing phosphor.

REFERENCES

[1] C. Zhang, L. Xiao, P. Zhong, and G. He, "Photometric optimization and comparison of hybrid white LEDs for mesopic road lighting," *Applied Optics*, vol. 57, no. 16, p. 4665, May 2018, doi: 10.1364/ao.57.004665.

[2] Z. Zhao, H. Zhang, S. Liu, and X. Wang, "Effective freeform TIR lens designed for LEDs with high angular color uniformity," *Applied Optics*, vol. 57, no. 15, p. 4216, May 2018, doi: 10.1364/ao.57.004216.

[3] J. X. Yang, D. S. Li, G. Li, E. Y. B. Pun, and H. Lin, "Photon quantification in Ho 3+ /Yb 3+ co-doped opto-thermal sensitive fluotellurite glass phosphor," *Applied Optics*, vol. 59, no. 19, p. 5752, Jun. 2020, doi: 10.1364/ao.396393.

[4] H. Lee, S. Kim, J. Heo, and W. J. Chung, "Phosphor-in-glass with Nd-doped glass for a white LED with a wide color gamut," *Optics Letters*, vol. 43, no. 4, p. 627, Feb. 2018, doi: 10.1364/ol.43.000627.

[5] W. Gao, K. Ding, G. He, and P. Zhong, "Color temperature tunable phosphor-coated white LEDs with excellent photometric and colorimetric performances," *Applied Optics*, vol. 57, no. 31, p. 9322, Oct. 2018, doi: 10.1364/ao.57.009322.

[6] Y. Tang, Z. Li, G. Liang, Z. Li, J. Li, and B. Yu, "Enhancement of luminous efficacy for LED lamps by introducing polyacrylonitrile electrospinning nanofiber film," *Optics Express*, vol. 26, no. 21, p. 27716, Oct. 2018, doi: 10.1364/oe.26.027716.

[7] Q. Guo *et al.*, "Characterization of YAG:Ce phosphor dosimeter by the co-precipitation method for radiotherapy," *Applied Optics*, vol. 60, no. 11, p. 3044, Apr. 2021, doi: 10.1364/ao.419800.

[8] H. Yuce, T. Guner, S. Balci, and M. M. Demir, "Phosphor-based white LED by various glassy particles: control over luminous efficiency," *Optics Letters*, vol. 44, no. 3, p. 479, Jan. 2019, doi: 10.1364/ol.44.000479.

[9] L. Yang, Q. Zhang, F. Li, A. Xie, L. Mao, and J. Ma, "Thermally stable lead-free phosphor in glass enhancement performance of light emitting diodes application," *Applied Optics*, vol. 58, no. 15, p. 4099, May 2019, doi: 10.1364/ao.58.004099.

[10] O. H. Kwon, J. S. Kim, J. W. Jang, and Y. S. Cho, "Simple prismatic patterning approach for nearly room-temperature processed planar remote phosphor layers for enhanced white luminescence efficiency," *Optical Materials Express*, vol. 8, no. 10, p. 3230, Oct. 2018, doi: 10.1364/ome.8.003230.

[11] J.-W. Shin *et al.*, "Overcoming the efficiency limit of organic light-emitting diodes using ultra-thin and transparent graphene electrodes," *Optics Express*, vol. 26, no. 2, p. 617, Jan. 2018, doi: 10.1364/oe.26.000617.

[12] T. Wu *et al.*, "Analyses of multi-color plant-growth light sources in achieving maximum photosynthesis efficiencies with enhanced color qualities," *Optics Express*, vol. 26, no. 4, p. 4135, Feb. 2018, doi: 10.1364/oe.26.004135.
[13] L. Li and M. J. Escuti, "Super achromatic wide-angle quarter-wave plates using multi-twist retarders," *Optics Express*, vol. 29, no. 5, p. 7464, Feb. 2021, doi: 10.1364/oe.418197.
[14] Y. Zhang, X. Zhu, A. Liu, Y. Weng, Z. Shen, and B. Wang, "Modeling and optimizing the chromatic holographic waveguide display system," *Applied Optics*, vol. 58, no. 34, p. G84, Oct. 2019, doi: 10.1364/ao.58.000g84.
[15] A. D. Corbett *et al.*, "Microscope calibration using laser written fluorescence," *Optics Express*, vol. 26, no. 17, p. 21887, Aug. 2018, doi: 10.1364/oe.26.021887.
[16] X. Ding *et al.*, "Improving the optical performance of multi-chip LEDs by using patterned phosphor configurations," *Optics Express*, vol. 26, no. 6, p. A283, Mar. 2018, doi: 10.1364/oe.26.00a283.
[17] A. R. Motschi *et al.*, "Identification and quantification of fibrotic areas in the human retina using polarization-sensitive OCT," *Biomedical Optics Express*, vol. 12, no. 7, p. 4380, Jun. 2021, doi: 10.1364/boe.426650.
[18] P. Liu *et al.*, "Laser regulation for variable color temperature lighting with low energy consumption by microlens arrays," *Applied Optics*, vol. 60, no. 19, p. 5652, Jun. 2021, doi: 10.1364/ao.425426.
[19] Q. Xu, L. Meng, and X. Wang, "Nanocrystal-filled polymer for improving angular color uniformity of phosphor-converted white LEDs," *Applied Optics*, vol. 58, no. 27, p. 7649, Sep. 2019, doi: 10.1364/ao.58.007649.
[20] S. S. Panda, H. S. Vyas, and R. S. Hegde, "Robust inverse design of all-dielectric metasurface transmission-mode color filters," *Optical Materials Express*, vol. 10, no. 12, p. 3145, Nov. 2020, doi: 10.1364/ome.409186.
[21] R. A. Deshpande, A. S. Roberts, and S. I. Bozhevolnyi, "Plasmonic color printing based on third-order gap surface plasmons," *Optical Materials Express*, vol. 9, no. 2, p. 717, Jan. 2019, doi: 10.1364/ome.9.000717.
[22] H. Daicho, K. Enomoto, H. Sawa, S. Matsuishi, and H. Hosono, "Improved color uniformity in white light-emitting diodes using newly developed phosphors," *Optics Express*, vol. 26, no. 19, p. 24784, Sep. 2018, doi: 10.1364/oe.26.024784.
[23] Q. Xu, B. Zhao, G. Cui, and M. R. Luo, "Testing uniform colour spaces using colour differences of a wide colour gamut," *Optics Express*, vol. 29, no. 5, p. 7778, Feb. 2021, doi: 10.1364/oe.413985.
[24] G. E. Romanova, V. I. Batshev, and A. S. Beliaeva, "Design of an optical illumination system for a tunable source with acousto-optical filtering," *Journal of Optical Technology*, vol. 88, no. 2, p. 66, Feb. 2021, doi: 10.1364/jot.88.000066.
[25] B. Yu *et al.*, "Luminous efficacy enhancement for LED lamps using highly reflective quantum dot-based photoluminescent films," *Optics Express*, vol. 29, no. 18, p. 29007, Aug. 2021, doi: 10.1364/oe.431345.
[26] R. Yoshimura, D.-H. Choi, M. Fujimoto, A. Uji, F. Hiwatashi, and K. Ohbayashi, "Dynamic optical coherence tomography imaging of the lacrimal passage with an extrinsic contrast agent," *Biomedical Optics Express*, vol. 10, no. 3, p. 1482, Feb. 2019, doi: 10.1364/boe.10.001482.
[27] J. Li *et al.*, "On-chip integration of III-nitride flip-chip light-emitting diodes with photodetectors," *Journal of Lightwave Technology*, vol. 39, no. 8, pp. 2603–2608, Apr. 2021, doi: 10.1109/JLT.2020.3048986.
[28] C.-M. Tsai, C.-S. Chang, Z. Xu, W.-P. Huang, W.-C. Lai, and J.-S. Bow, "Efficiency enhancement of III-nitride light-emitting diodes with strain-compensated thin-barrier InGaN/AlN/GaN multiple quantum wells," *OSA Continuum*, vol. 2, no. 4, p. 1207, Mar. 2019, doi: 10.1364/osac.2.001207.

BIOGRAPHIES OF AUTHORS

Ho Minh Trung received the Ph.D. degree in physics from University of Science, Vietnam National University Ho Chi Minh City, Vietnam. He is working as a lecturer at the faculty of basic sciences, Vinh Long University of Technology Education, Vietnam. His research interests focus on developing the patterned substrate with micro- and nano-scale to apply for physical and chemical devices such as solar cells, OLED, photoanode. He can be contacted at email: trunghm@vlute.edu.vn.

My Hanh Nguyen Thi received a bachelor of physics from an Giang University, Vietnam, master of theoretical physics and mathematical physics, Hanoi National University of Education, Vietnam. Currently. She is a lecturer at the faculty of mechanical engineering, Industrial University of Ho Chi Minh City, Vietnam. Her research interests are theoretical physics and mathematical physics. She can be contacted at email: nguyenthimyhanh@iuh.edu.vn.

Nguyen Le Thai received his BS in electronic engineering from Danang University of Science and Technology, Vietnam, in 2003, MS in electronic engineering from Posts and Telecommunications Institute of Technology, Ho Chi Minh, Vietnam, in 2011 and Ph.D. degree of mechatronics engineering from Kunming University of Science and Technology, China, in 2016. He is a currently with the Nguyen Tat Thanh University, Ho Chi Minh City, Vietnam. His research interests include the renewable energy, optimisation techniques, robust adaptive control and signal processing. He can be contacted at email: nlthai@nttu.edu.vn.